

STM study of oligo(phenylene-ethynylene)s

This content has been downloaded from IOPscience. Please scroll down to see the full text.

2015 New J. Phys. 17 053043

(<http://iopscience.iop.org/1367-2630/17/5/053043>)

View [the table of contents for this issue](#), or go to the [journal homepage](#) for more

Download details:

IP Address: 141.52.96.80

This content was downloaded on 19/06/2015 at 09:24

Please note that [terms and conditions apply](#).



PAPER

STM study of oligo(phenylene-ethynylene)s

OPEN ACCESS

RECEIVED

27 November 2014

REVISED

9 March 2015

ACCEPTED FOR PUBLICATION

29 April 2015

PUBLISHED

27 May 2015

Content from this work
may be used under the
terms of the [Creative
Commons Attribution 3.0
licence](#).

Any further distribution of
this work must maintain
attribution to the
author(s) and the title of
the work, journal citation
and DOI.



Cornelius Thiele^{1,2}, Lukas Gerhard¹, Thomas R Eaton³, David Muñoz Torres³, Marcel Mayor^{1,2,3},
Wulf Wulfhekel^{1,2,4}, Hilbert v Löhneysen^{1,2,4} and Maya Lukas¹

¹ Institute of Nanotechnology, Karlsruhe Institute of Technology, D-76021 Karlsruhe, Germany

² DFG Center for Functional Nanostructures (CFN), D-76028 Karlsruhe, Germany

³ Department of Chemistry, University of Basel, 4056 Basel, Switzerland

⁴ Physikalisches Institut, Karlsruhe Institute of Technology, D-76128 Karlsruhe, Germany

E-mail: Lukas.Gerhard@kit.edu

Keywords: molecular wire, scanning tunneling microscopy, molecular resolution, single molecule conductance

Supplementary material for this article is available [online](#)

Abstract

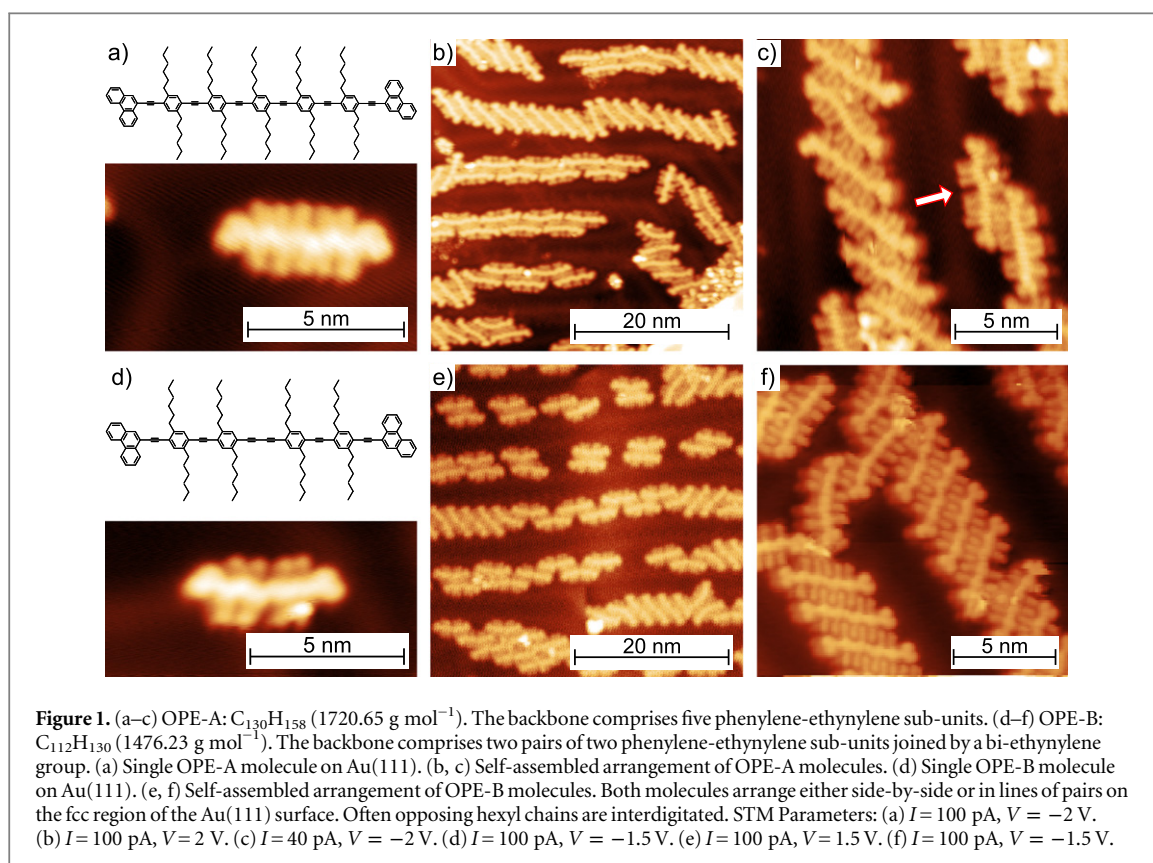
A detailed scanning tunneling microscopy (STM) study of two variants of oligo(phenylene ethynylene) (OPE) molecules is presented. These molecules might serve as molecular wires up to ≈ 5 nm in length. Self-assembled arrangements as well as single molecules on a Au(111) surface were analyzed. The molecular orbitals were directly imaged and are compared to density functional theory calculations. Sub-molecular resolution images of both molecules directly display the chemical structure. One of the OPE variants was lifted off the surface by the STM tip to measure the single-molecule conductance in order to explain previously reported low conduction values. Furthermore, we present a detailed analysis of a tip-induced conformational switching of the hexyl side groups from all-trans to a nonlinear conformation, which was observed for both variants.

1. Introduction

Knowledge of electronic properties and conformation of a molecule attached to metallic electrodes is essential for its integration into a functional molecular electronic device. With regard to possible applications in those devices, it is of crucial importance to understand how a metallic substrate affects the properties of a molecular building block. This holds all the more for larger and more complex molecules with their much larger degree of freedom in conformation and bonding configurations compared to smaller compact molecules.

Conformational changes that are induced by electron transport through such molecules might on the one hand be used to realize electronic function. They might on the other hand at the same time occur as an undesired side-effect. In both cases, knowledge of these processes and their effect on the electronic properties of the molecule is crucial for the design of molecular electronic units. Oligo(phenylene ethynylene)s (OPEs) have been discussed as candidates for molecular wires since the early nineties [1–6]. While there has been tremendous progress in the synthesis of these molecular wires over the last decade, enabling complex U-shaped, kinked and cyclic geometries [7–9], the physical properties of these wires are not yet well understood calling for a more detailed study. Although similar molecules have been extensively studied in break junctions [10, 11], scanning-probe studies of OPE molecules have so far been limited to the self-assembled monolayers (SAMs) of OPEs or OPEs inserted into SAMs of other molecules [12–18] while the adsorption of single, isolated OPE molecules has not been studied at all. Density functional theory (DFT) studies of OPEs reported on the effect of central-group substituents [19] or various terminal groups [20] on the molecular orbitals and the electronic properties. However, theoretical calculations have not been tested against experimental data.

In the present work we focus on two comparable OPE-type molecules, namely the OPE pentamer comprising terminal 9-yl-phenantrene groups entitled OPE-A (see figure 1(a)) and the slightly shorter analog OPE-B in which the central para-phenyl unit is missing (see figure 1(d)). Recently, OPE-A molecules were contacted using carbon nanotube nanogap electrodes [21] and unexpectedly high resistances on the order of $90\text{G}\Omega$ were observed in spite of their fully conjugated structure. In order to gain new insights into the electronic



structure of the molecule at the sub-nanometer scale, its conduction under well controlled geometries and the complex interplay of the molecule with the metallic leads, we performed a detailed scanning tunneling microscopy (STM) study. Spectroscopic measurements and tunneling-conductance maps of the molecular orbitals were obtained on both self-assembled arrangements and single molecules adsorbed on a Au(111) single-crystal surface. These measurements of the electronic structure are compared to DFT calculations. Contrary to the naive prediction of high conductive conjugated bonds, the molecule deforms upon adsorption such that the conjugated bonds are bend and twisted, explaining the low conduction. Further, the energetic positions of the molecular orbitals are not in favour of high conductivity at low bias. For a direct comparison with our previous work, we measured the conductance of the molecule when partially lifted off the surface. Finally, we observed an electron-induced conformational switching of the molecule which we explain by a transition from the all-trans state to a different conformation of the hexyl chain. This indicates a large number of molecular degrees of freedom even when the molecule is adsorbed in a metallic junction and indirectly affects the conductance along the molecular backbone as it acts on the torsion angles between the phenyl groups [22].

2. Methods

2.1. Sample preparation

A home-built liquid-helium cooled ultra-high vacuum (UHV) STM equipped with a Femto preamplifier and a Nanonis control system was used in this work. First, a clean Au(111) single-crystal surface was prepared by several cycles of argon-ion sputtering and annealing to 770 K in UHV. STM tips were electrochemically etched from tungsten wires and cleaned on the Au(111) surface by repeated voltage pulses and gentle crashes. During molecule deposition, the Au crystal (surface area $\approx 4 \times 6 \text{ mm}^2$) was briefly exposed to atmospheric conditions in the load-lock. Au(111) surfaces with single adsorbed organic molecules were prepared by dissolving the molecule in dichloromethane (DCM, CH_2Cl_2) and then allowing a drop of the solution to dry on the Au(111) surface. The molecular concentration was $\approx 5 \times 10^{-7} \text{ mol l}^{-1}$. DCM was chosen as solvent because earlier studies had shown that it is possible to almost completely remove it from a Au(111) surface by gentle heating in UHV [23]. For all solutions high-purity DCM was obtained by distilling HPLC-grade DCM twice in a clean still. The volume of the drop was $\approx 8 \mu\text{l}$ and its evaporation typically took no longer than 20 s. The load-lock was then evacuated and the crystal transferred back into the UHV chamber where it was annealed at 400 K to promote the desorption of DCM, and then transferred to the pre-cooled STM. All STM images were recorded with a constant

sample temperature of ≈ 5 K and in constant-current mode (called topographic images in the following), if not indicated otherwise. dI/dV images (conductance maps) were recorded by additionally measuring dI/dV for each image point with a lock-in amplifier (typical STM parameters: $I = 200$ pA, $f_{\text{osc}} = 1.33$ kHz, $A_{\text{osc}} = 42$ mV).

The backbone of OPE-A consists of five phenylene-ethynylene sub-units whereas the backbone of OPE-B features two pairs of two sub-units joined in the center by a bi-ethynylene group. Two hexyl chains are attached at the phenylene groups of each sub-unit to promote solubility in organic solvents. Both molecules feature phenanthrene anchor groups on each end to allow π - π coupling to the sidewall of carbon nanotubes [24, 25] for our direct-contacting experiments. While OPE-A resembles a straight wire, the integration of the bi-ethynylene group at its center makes OPE-B resemble a junction of two shorter wires. Both molecules were synthesized by performing a series of acetylene protection and deprotection steps, similar to synthesis of the molecule used by Grunder *et al* [26, 27]. Full synthetic details for OPE-A can be found in the supplementary material of [21].

2.2. Density functional theory

To compare the spectroscopic data with theoretical calculations, DFT calculations were performed with the program *TURBOMOLE v6.4* [28]. The multipole-accelerated resolution of identity approximation was used throughout. The self-consistent-field energy was converged to 10^{-6} for structure optimizations, with a grid-size setting of *m4*. For calculations of molecules in the gas phase, the 6–31 g^* basis set [29] and the B3LYP [30] functional were chosen, which are typical choices for conjugated organic molecules [19, 31, 32]. To investigate hybridization effects of the molecular orbitals with the conductive surface, a closely packed layer of gold atoms, representing an unreconstructed Au(111) surface, was included in a DFT calculation for a smaller version of the OPE-A molecule (see supporting information). To reduce the computational requirements of these calculations, the BP86 functional [33, 34] and the def-SVP basis set [35, 36] were used. van der Waals interactions were incorporated into the calculations by the DFT-D3 approximation with Becke–Johnson damping [37, 38].

3. Results

3.1. Single molecules and self-assembly

Both OPE-A and OPE-B arrange in regular patterns on the gold surface (see figures 1(b), (c) and figures 1(e), (f)). They reside preferentially on the face-centered-cubic region of the Au(111) reconstruction indicating a stronger molecule-surface interaction on fcc stacked regions than on hcp regions. In both cases the molecules arrange side-by-side or in lines of pairs and adsorb flat on the surface, i.e., the benzene rings of the phenylene and phenanthrene groups are aligned parallel to the surface. The five (two times two) hexyl chains of OPE-A (OPE-B) protrude from each side of the molecule. In many cases the alkyl chains of opposing molecules are interdigitated indicating an attractive intermolecular interaction that overcomes the steric repulsion [39].

The sub-units of a molecule can rotate against each other at single bonds in solution. As the hexyl chains are attached asymmetrically to the phenylene groups, the observed distance between neighboring chains of an individual molecule varies when its sub-units are not in the same rotational conformation, as pointed out in figure 1(c) by an arrow. Also, the rotation of the phenanthrene anchor groups leads to two asymmetric forms on the surface. These different conformations can clearly be inferred from constant-current images. Additionally, while most OPE-A and OPE-B molecules exhibit a straight configuration on the surface, the molecule's backbone was observed to occasionally bend strongly, despite its supposedly rigid structure [1]. This is attributed to a strong interaction with the substrate with relatively deep adsorption minima and is one reason for unexpectedly low conductance values of the molecule.

By lowering the molecular concentration in the deposition drop to $\approx 1 \times 10^{-8}$ mol l $^{-1}$, isolated single molecules on the Au surface are observed. Typically, only a few molecules were then found per Au(111) terrace, with roughly half of the surface covered by islands of solvent residue. The molecules tend to arrange in pairs or triples even at this very low concentration, which suggests a high mobility on the Au(111) surface at annealing temperatures of 400 K. They often freeze out in a side-by-side arrangement upon cooling, as shown in figure 2(a). The energy landscape of the Au(111) surface is not entirely structureless [40, 41]: the 'elbow' sites of the reconstruction offer the lowest electron binding energies on the surface, followed by the fcc regions. Consequently, single molecules and isolated pairs were often observed at these 'elbow' sites, and self-assembled arrangements of OPE-A and OPE-B molecules were typically found on the fcc regions of the surface.

By positioning the STM tip above the anchor group of a molecule and increasing the current to 2 nA, it was possible to drag an OPE-A molecule by the STM tip, see figure 2. When the current was again decreased to the usual imaging levels of ≈ 50 pA, the molecule could be imaged at its new position. With a suitable tip, molecules could be freely moved on a Au(111) terrace, even across transition regions of the surface reconstruction. As shown in the consecutive images in figure 2, it was thus possible to pull apart a pair of molecules, thus isolating

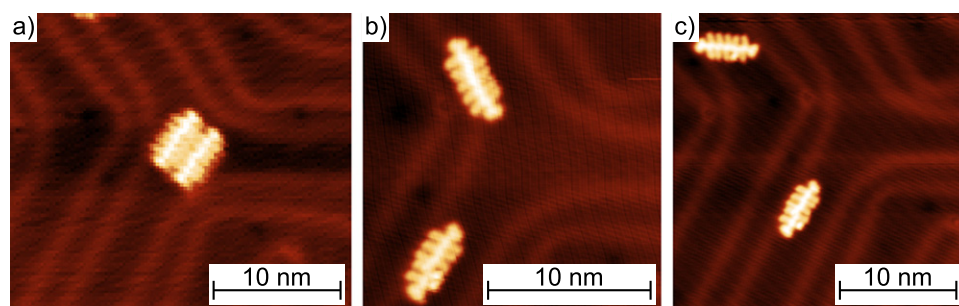


Figure 2. Separating a pair of OPE-A molecules by dragging them with the STM tip. The tip is positioned above the anchor group and the current increased to ≈ 2 nA. When the tip is moved, the molecule follows in the wake of the tip's electric field. Images were taken after these pulling steps. STM parameters: (a) $I = 50$ pA, $V = 1.5$ V. (b) $I = 40$ pA, $V = 1.5$ V. (c) $I = 50$ pA, $V = 1.5$ V.

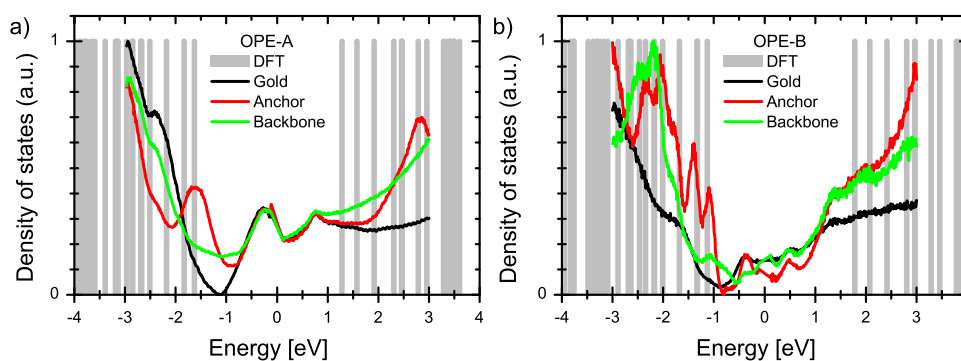


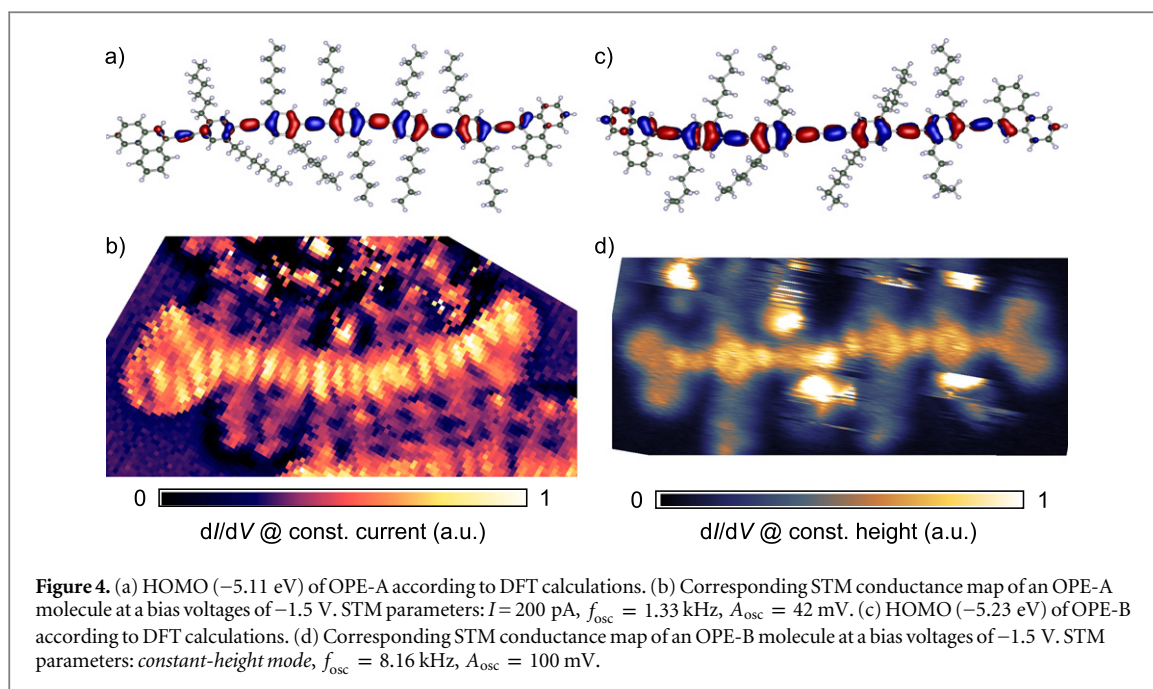
Figure 3. Comparison of spectroscopic measurements and results of DFT calculation according to def-SVP/B3LYP level of theory for (a) OPE-A and (b) OPE-B. Plotted is the averaged $(dI/dV)/(I/V)$ signal above various positions of the molecule and the clean gold surface. Gray bars correspond to energies of molecular orbitals from the DFT calculation. The DFT energies were shifted by (a) 3.41 eV (b) 3.68 eV to align the energy of the highest occupied molecular orbital from DFT and spectroscopy.

them. We suspect this effect is driven by the high electric field gradients generated by a sharp STM tip. The molecules did not follow STM tips that appeared to be blunt, even at higher tunneling currents of up to 100 nA. By another technique, described by Jung *et al* [42] it proved possible to move molecules on the surface independent of the shape of the STM tip: the feedback loop was disabled and the STM tip moved closer to the surface in the vicinity of a molecule. Then, the tip was moved laterally over the molecule. Eventually, repulsive forces between the tip and the molecule pushed it away from the tip, roughly in the direction of tip movement.

3.2. Scanning tunneling spectroscopy

In order to investigate the electronic structure and to further understand the electronic transport, spectroscopic measurements were carried out with the tip placed at well-defined locations above a molecule. The position was fixed (always maintaining a vacuum gap between tip and sample), and the voltage was swept from $V = -3$ to 3 V while the dI/dV signal was simultaneously recorded with a lock-in amplifier. Positive bias voltages probe unoccupied states of the sample, whereas negative voltages probe occupied states. Spectra on the clean gold surface were acquired for comparison. Any peaks in the spectra of the molecule-covered surface that also were seen in the Au spectra are obviously due to the gold or the tip but not due the molecule and therefore are discarded in the following discussion (e.g., the Au(111) surface state at ≈ -470 mV). Spectroscopic data above the backbone of both molecules as well as above their anchor groups were recorded. The normalized $(dI/dV)/(I/V)$ signal is interpreted as the density of states and plotted in figure 3.

For OPE-A, spectra above the anchor group display at negative voltages a pronounced peak at ≈ -1.6 V. No additional peak is observed at negative voltages. For positive voltages, a steady increase of the density of states up to a peak at ≈ 2.8 V is observed. Concerning OPE-B, several peaks can be identified above the anchor group for negative voltages at ≈ -1.2 V, ≈ -1.4 V, ≈ -2 V and ≈ -2.3 V. With the tip above the backbone, a small peak of the density of states is observed at ≈ -1.2 V as well, with the density of states subsequently decreasing, then increasing to another peak at ≈ -2.2 V. For unoccupied states, a peak at ≈ 2 V in the density of states is observed. For both molecules, pronounced peaks in the density of states are observed for negative voltages. From ultraviolet–visible fluorescence measurements on solutions of OPE-A and OPE-B in DCM, we extract an energy



gap of 2.95 eV for OPE-A and 2.90 eV for OPE-B in full agreement with measurements on similar molecules [43]. Due to a solvatochromic shift from the polarizability of the surrounding solvent, these values are not expected to correspond to the energy gaps of the free molecules. Likewise, hybridization with surface states affects the molecular orbitals. For both molecules, the energetic position of the lowest unoccupied molecular orbital (LUMO) is difficult to precisely ascertain from the STM spectra, but the obvious lack of molecular orbitals at low energies corroborates the experimentally obtained low conductance values.

DFT calculations of the molecules in the gas phase yield energy gaps of 2.85 eV for OPE-A and 2.91 eV for OPE-B. A comparison of near-gap orbital energies from the DFT calculations with the spectroscopic data is shown in figure 3. To directly observe the location and shape of molecular orbitals, tunneling conductance maps (dI/dV images) of both molecules were recorded at various bias voltages and compared to the calculated molecular orbitals (see figure 4). Due to hybridization of molecular orbitals with surface states and the resulting finite electronic lifetimes of the orbitals, it is typically only possible to observe a convolution of different, energetically closely spaced orbitals. Orbitals with three lobes per phenylene-ethynylene sub-unit are observed in the experimental conductance maps of both molecules at bias voltages of -1.5 V (figures 4 (b) and (d); further dI/dV images are shown in figure S1 (available at stacks.iop.org/njp/17/053043/mmedia). These elliptical lobes are centered along the backbone of the molecule. We attribute these lobes to the highest occupied molecular orbitals (HOMOs), in agreement with our spectroscopic data, where the first peaks attributed to occupied molecular orbitals were observed in the same voltage range. The experimental conductance maps are compared to the shapes of the HOMOs according to gas phase DFT calculations in figures 4 (a) and (c). We find a good agreement, which indicates that, in our case, the hybridization of the HOMO proved for both molecules sufficiently weak to allow observation almost unconvoluted. The different elliptical shapes of the individual lobes are only observed for OPE-B molecules, which we attribute to a tip effect. The exact shapes depend on the side chains of the central sub-units as well as on their torsion angle. For planar configurations, delocalized orbitals are found for both the LUMO and the HOMO [19, 31], with similar shapes as in our calculations. Since the experimental conductance maps of the HOMO of OPE-A (OPE-B) at $U = -1.5$ V correspond very well to the shapes of the orbitals in our DFT calculations of the respective HOMO, we align the energy scale of the DFT calculation and the STS spectra at the energy of the respective HOMO (see figure 3). The DFT energies were shifted by 3.41 eV and 3.68 eV for OPE-A and OPE-B, respectively.

Imaging of the unconvoluted LUMOs proved difficult for both molecules, presumably because the hybridization of these orbitals with the surface is stronger, see figure S1. To investigate the hybridization of the molecular orbitals with the conductive surface, DFT calculations including a slab of the Au surface were conducted. For computational issues a shortened OPE molecule was used (see figure S2). The HOMO orbital did not hybridize with the surface, while the LUMO was split into several states and showed strong hybridization with surface states in accordance with our experimental findings. At a bias voltage of -2.5 V, it was possible to record the shape of occupied states below the HOMO of an OPE-A molecule. From the DFT calculation, this

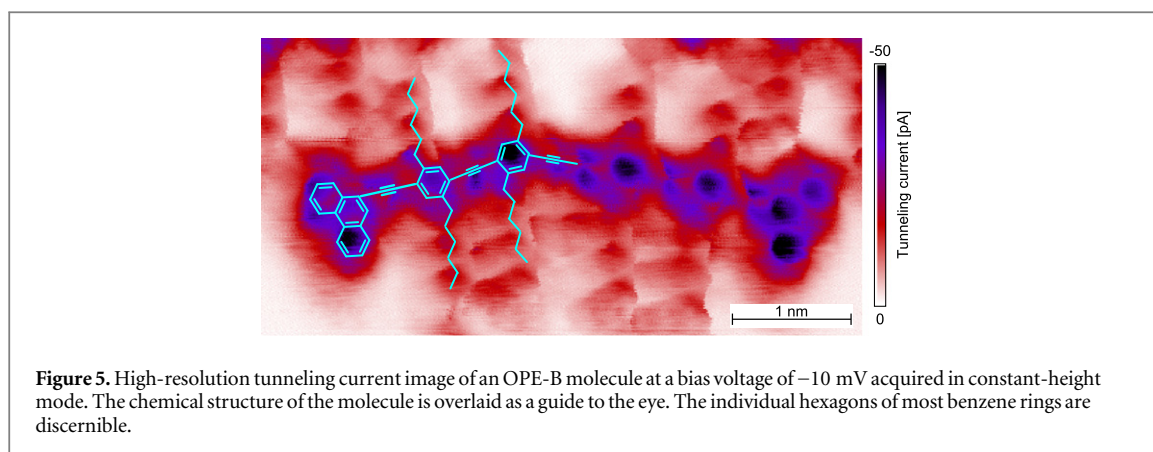


Figure 5. High-resolution tunneling current image of an OPE-B molecule at a bias voltage of -10 mV acquired in constant-height mode. The chemical structure of the molecule is overlaid as a guide to the eye. The individual hexagons of most benzene rings are discernible.

shape can be constructed by the sum of four nearly degenerate states with energies of 1.52 – 1.63 eV below the HOMO energy. A side-by-side comparison of the DFT results and the conductance map is shown in figure S3.

3.3. Sub-molecular resolution imaging

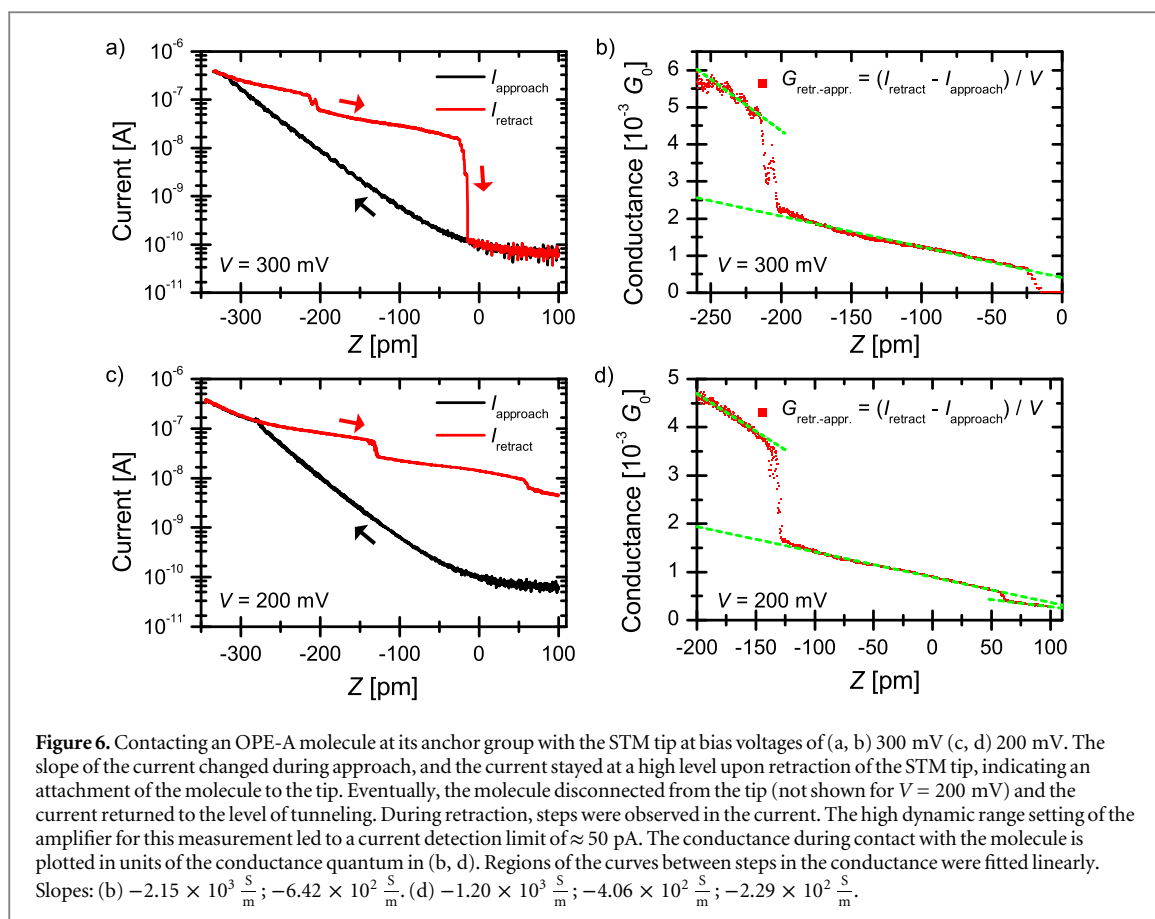
Since its invention, the STM has been capable of resolving surfaces with atomic resolution. However, atomic resolution imaging of individual adsorbed molecules seemed to be out of reach because the topographic contrast of the STM is based on the local density of electronic states, i.e., the molecular orbitals, which need not be correlated with a molecule's chemical structure. Recently, non-contact atomic force microscopy (ncAFM) [44, 45] and scanning tunneling hydrogen microscopy [46] (STHM) have been reported to achieve atomic resolution of single organic molecules, i.e., direct images of a molecule's chemical structure. STHM data has been reported for 3,4,9,10-perylene-tetracarboxylic dianhydride (PTCDA) monolayers and pentacene molecules on Au(111) [46–48]. For STHM on PTCDA, a favorable interaction of a hydrogen atom at the apex of the STM tip with the molecule has been proposed as the cause of the resolution enhancement [49]. The underlying contrast mechanism may also be related to Pauli repulsion [47].

By using bias voltages well inside the energy gap it was possible to observe OPE-A and OPE-B at sub-molecular, near-atomic resolution. For a high-resolution image of OPE-B obtained in constant-height mode at a bias voltage of -10 mV, see figure 5. The individual hexagons of the carbon rings on the backbone and in the anchor groups can be seen. The tunneling current is highest above the center of a benzene ring, and decreases sharply above the assumed positions of carbon atoms and covalent bonds between them. For the ethynylene groups along the backbone of the molecule, the highest current was observed on a cone-shaped area protruding from each side of the group. Similarly, in constant-current mode, at a set point of 90 pA and bias voltages between 100 and 200 mV, the individual benzene rings of OPE-A can be identified in the dI/dV image, see figure S4. The benzene rings along the backbone, as well as the three benzene rings of the anchor group, are clearly visible. The topographic image recorded simultaneously does not exhibit these features. The observed contrast is similar to the STHM contrast reported by Temirov *et al* on PTCDA and tetracene molecules on a metal surface. Such high-resolution STM images of organic molecules provide a fascinating insight into the structure and may fuel detailed theoretical studies on the origin of this imaging contrast.

3.4. In situ contacting

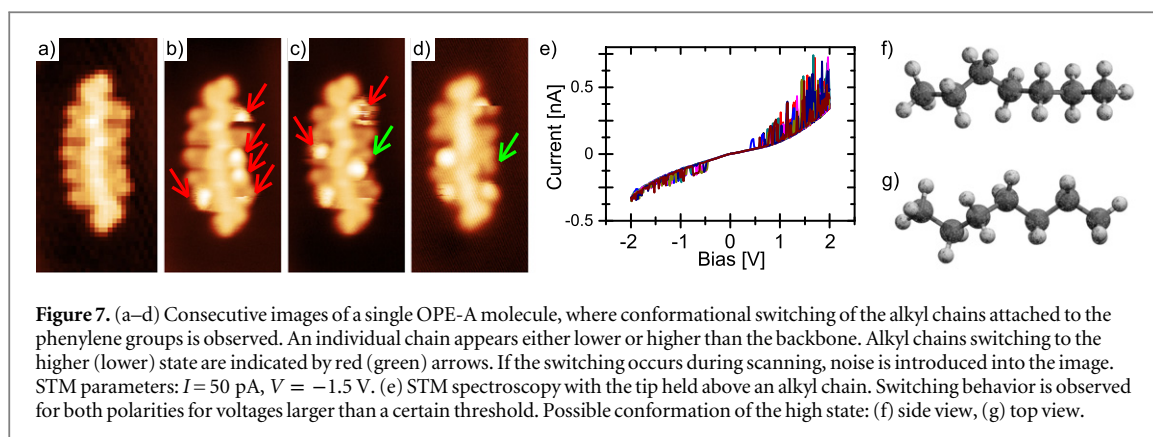
As discussed in section 3.2, OPE molecules were conceived as molecular wires with the purpose to carry an electric current. In addition to investigating the local electronic structure of the molecules by local dI/dV spectra and conductance images, therefore, efforts were undertaken to directly contact and lift off OPE-A molecules with the STM tip in order to measure the conductance of the thus contacted wire. To this end, the tip was positioned above one of the anchor groups and then lowered towards the surface. The molecule eventually attaches to the tip upon approach and can be pulled upwards from the surface upon retraction. The measured current during retraction typically exceeds that of mere tunneling, as long as the molecule acts as a conductive bridge between tip and surface. When the molecule disconnects from the tip and falls back to the surface the current abruptly decreases to the value of the approach curve (tunneling) [50, 51].

Such approach-retract curves at bias voltages of 300 and 200 mV are plotted in figures 6(a) and (c). Before lowering the tip towards the anchor group, the tunneling current was stabilized at 100 pA with the feedback loop active. The corresponding height defines the zero point of the height scale of the approach-retract curves. The feedback loop was then disabled and the tip first retracted by 100 pm, before the approach was started. At this point ($Z = 100$ pm) the current was below the detection limit of ≈ 50 pA, as a high dynamic range setting on the



amplifier was used for contacting experiments. The tip was then lowered towards the surface until a current of ≈ 400 nA was recorded. Then, the tip was retracted again. Initially, the current increased exponentially during approach, from $Z = 0$ to $Z \approx -300$ pm (-275 pm for 200 mV bias). A change in the slope of the current-distance curve indicates that the STM tip has come into contact with the anchor group. Upon retraction of the STM tip, the current stayed at a high level, with small steps observed in the current. Eventually, upon disconnection of the molecule from the STM tip, the current fell back to the vacuum tunneling level (not shown for a bias voltage of 200 mV). A molecule typically disconnected earlier from the STM tip when using higher bias voltages.

The current upon approach was subtracted from the current upon withdrawal to yield only the current flowing through the molecule. The conductance $G_{\text{retr-appr}} = (I_{\text{retr}} - I_{\text{appr}})/V$ for both approach-retract curves is plotted in figures 6(b) and (d) in units of the conductance quantum $G_0 = \frac{2e^2}{h} = 7.748 \times 10^{-5}$ S. For a bias voltage of 200 mV (figure 6(d)), three regions of the curve, separated by steps in the conductance, were found. The conductance decreased at these steps from $3.69 \times 10^{-3} G_0$ to $1.67 \times 10^{-3} G_0$ and from $0.63 \times 10^{-3} G_0$ to $0.39 \times 10^{-3} G_0$, respectively. Our interpretation of these steps is, that one part of the molecule's length will detach from the gold surface after the other so that the molecular wire is 'peeled off' the surface by a sequence of discrete events. With each detached group the length of the freely suspended wire between the two electrodes increases leading to an abrupt drop of the conductance. Thus the conductance of the plateaus between steps might be constant—in contrast to the observed linear dependence of the conductance on the withdrawal distance. Possibly, a distortion of the molecule gradually reduces the transmission coefficient of the conductance channels of the molecular backbone [52, 53]. The recorded slopes are similar for 200 and 300 mV bias, ranging from -1.20×10^3 to $-2.29 \times 10^2 \text{ Sm}^{-1}$ and from -2.15×10^3 to $-6.42 \times 10^2 \text{ Sm}^{-1}$. The similar step heights and slopes suggest that in both lifting processes the same parts of the molecule are detached from the surface. Near the maximum extension, resistance values of $\approx 50 \text{ M}\Omega$ were observed, which at first sight appears to be large compared to values known from other molecules. However, our STS measurement revealed a gap of about +1 to -1.6 eV so that at the contacting voltage of 200 to 300 mV contribution of the HOMO and LUMO orbitals to the conduction is negligible. The low conductance values are in full agreement with conductance measurements in STM break-junction experiments where a resistance of a similar OPE molecule of $\approx 200 \text{ M}\Omega$ was reported [43]. In our STM experiments we were not able to stretch the molecular bridge to its full length and a large portion of the molecule (total length $\approx 50 \text{ \AA}$) was always still in contact with the gold surface. The reason

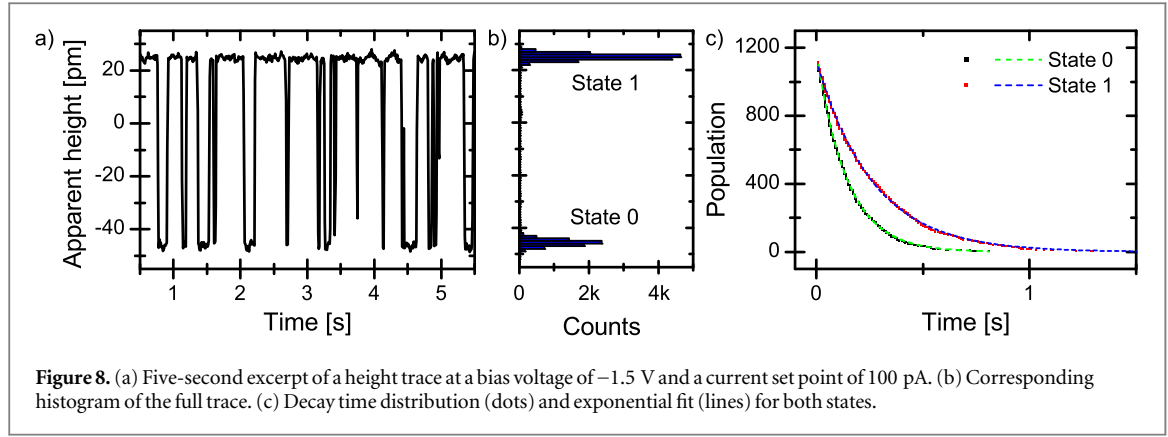


probably is that our tip became covered with gold during the tip shaping process but has a smaller contact area with the molecule than the substrate. Thus, the binding forces between tip and molecule are smaller than those between molecule and substrate. It is reasonable to assume that the resistance of a single molecule would be even higher when contacted only by its anchor end groups. Indeed, in our contacting experiments with carbon nanotube nanogap electrodes [21] we found an average resistance of $90 \text{ G}\Omega$ with OPE-A molecules in the junction. We attributed the remaining discrepancy in resistance to the different kind of contact electrodes and the uncontrolled placement of OPE-A molecules in the nanotube nanogap. Furthermore, as mentioned above, our STM experiments revealed that the molecules have a tendency to strongly bend on the surface, which might happen to a molecule suspended between two contacts as well. The resulting distortion is expected to reduce the conductivity of the molecule, as DFT calculations on OPE molecules [20, 53] and experiments on biphenyl molecules [22, 52] have shown that any bending or torsion of the backbone sub-units decreases the conductance significantly.

4. Conformational switching of alkyl chains

As discussed in sections 3.2 and 3.4 the conformation of the alkyl chains and the torsion angle between the sub-units of the backbone determines the exact structure of the orbitals of the backbone and accordingly its conductance [19, 31]. Placing the molecule on the surface, the conformation of side chains will inevitably affect the torsion angle between the sub-units of the backbone as well. For the use as a reliable molecular wire, the side chains of the backbone need to be in a stable conformation throughout the parameter range in which the conductor is used. When the molecule is freshly deposited, the alkyl chains lie flat on the surface. However, sequential images of a single molecule revealed that the alkyl chains attached to each side of the phenylene groups of OPE-A and OPE-B are not fixed in their conformation. By performing a detailed scan of the molecule, thereby increasing the interaction time between STM tip and molecule, switching between two bistable conformations can be induced. In the topographic image, an alkyl chain thus appears either closer or more distinct from the tip than the backbone. Figures 7(a)–(d) shows four consecutive images of a single OPE-A molecule where this switching behavior has occurred. The difference in height of ≈ 70 pm can be explained by the rotational conformation presented in figures 7(f) and (g). Spectroscopic measurements with the tip held above an alkyl chain are complicated by switching events, as the tunneling current fluctuates as soon as a certain threshold in bias voltage is reached, see figure 7(e). The threshold voltage appears to be of the same magnitude for positive and negative bias.

The first STM observation of bistable switching was reported by Eigler *et al* in 1991, where a xenon atom moved back and forth between the STM tip and a Ni surface [54]. The transition rate between the two states showed a power-law dependence on the tunneling current, which was attributed to stepwise vibrational heating due to inelastic electron scattering [55–57]. Conformational switching of a single organic molecule between two states was reported for OPEs embedded in a dodecanethiol monolayer [58]. The switching occurred during scanning, and in some cases could be induced by pulsing the electric field above a molecule. A linear dependence of the transition rate on the current as well as an exponential distribution of residence times in the individual states is expected for statistically independent one-electron processes [59, 60]. Neglecting temperature and lifetime broadening of the inelastic tunneling rate, the transition rate Γ is then approximately proportional to the conductance G and the effective electron–vibron coupling strength λ [56, 61]:



$$\Gamma_{0,1}(V) \cong \frac{\lambda G}{e} (|V| - V_{\text{th},0,1}) \Theta(|V| - V_{\text{th},0,1}), \quad (1)$$

with the Heaviside step function Θ and the threshold voltage $V_{\text{th},0}$ for switching from state 0 to state 1 and $V_{\text{th},1}$ for switching from state 1 to state 0. We observed only two stable current levels with the STM tip held above an alkyl chain. The conductance ratio between these two states and the transition rate depend on the exact position of the tip relative to the molecule. To further analyze the mechanism of the conformational switching, height traces above an alkyl chain were recorded in constant-current mode at different tunneling currents and bias voltages. Traces were recorded with a sampling rate of 20 or 50 ms and a length up to 20 min, until a reasonable amount of switching events (>100) were observed for each parameter combination. A five-second excerpt of one of these traces is plotted in figure 8(a), for a bias voltage of -1.5 V and a tunneling current of 100 pA. Two height levels with a difference of ≈ 70 pm can be identified. Consequently, the data were discriminated into two states, 0 and 1. In state 0, the alkyl chain appears flat on the surface, while in state 1 it appears higher than the backbone. The corresponding histogram of apparent heights for the full trace is plotted in figure 8(b).

The residence times $\tau_i^{(0,1)}$ in each state were extracted from the time traces and averaged to obtain the mean lifetime of each state $\bar{\tau}^{(0/1)}$:

$$\bar{\tau}^{(0,1)} = \frac{1}{N} \sum_{i=1}^N \tau_i^{(0,1)}. \quad (2)$$

The error on this lifetime is the standard deviation of the mean:

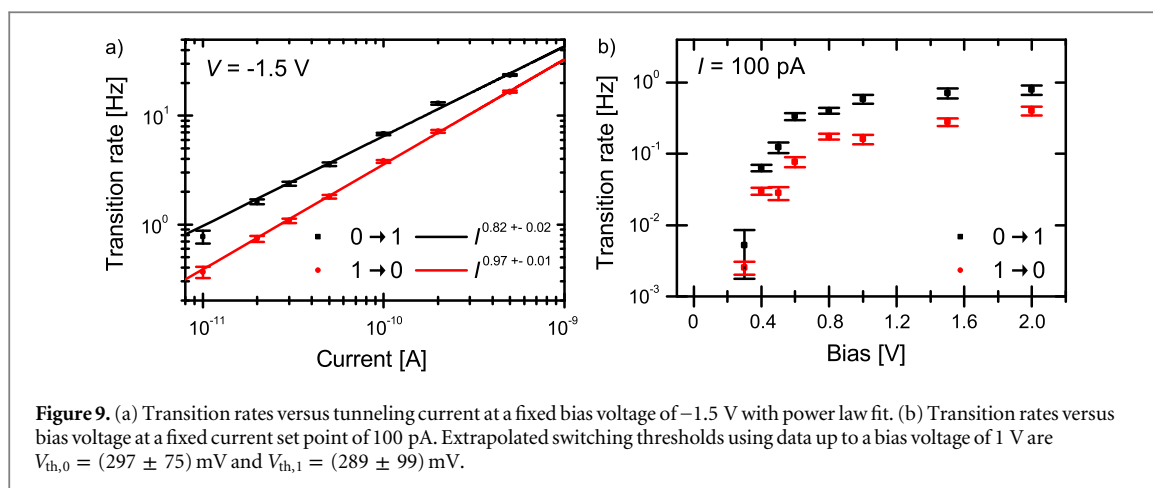
$$\sigma_{\bar{\tau}^{(0,1)}} = \sqrt{\frac{\sum_{i=1}^N (\tau_i^{(0,1)} - \bar{\tau}^{(0,1)})^2}{N(N-1)}}. \quad (3)$$

Using the extracted lifetime and the number of switching events as a state's initial population $N_0^{(0,1)}$, exponential decay functions $N^{(0,1)}(t) = N_0^{(0,1)} e^{-t/\bar{\tau}^{(0,1)}}$ can be constructed that fit the data well (see figure 8(c)). This analysis was performed for all recorded traces.

The transition rates for a bias voltage of -1.5 V, $\Gamma_{0,1} = 1/\bar{\tau}^{(0,1)}$, are plotted versus current in figure 9(a) on a double-logarithmic plot. From power-law fits with $\Gamma_{0,1} \propto I^n$ exponents of 0.82 ± 0.02 and 0.97 ± 0.01 are obtained, i.e., the transition rate is roughly proportional to the current. This implies that the transition is a single-electron process. To extract the switching threshold voltage from our data, we plot the transition rate at a constant current set point versus bias voltage, see figure 9(b). From linear fits including data points up to 1 V, the threshold voltages for the two states are $V_{\text{th},0} = (297 \pm 75)$ mV and $V_{\text{th},1} = (289 \pm 99)$ mV. Thus the switching is expected to be caused by a single electron process with an energetic barrier of ≈ 300 meV. This energy is in the range of C–H stretching modes which are softened in the vicinity of the Au(111) surface and which are of the order of 2800 cm^{-1} or 350 meV [62]. With bias voltages below 300 mV, switching events could not be observed for reasonable observation times. These findings allow using the bistable conformational state as a memory bit: writing involves waiting for the conformation to switch into the desired state at a higher bias voltage. The state can then be read out at lower bias voltages.

5. Summary

STM measurements of the electronic structure of single, isolated OPE molecules on a Au(111) surface were presented. Both OPE variants we studied tend to arrange in regular patterns on the fcc regions of the



reconstructed Au(111) surface. At lower molecular concentrations, molecules were still mostly grouped in pairs or triples, which suggests they diffuse during the surface preparation at temperatures of 400 K and an attraction by intermolecular forces. Despite the influence of the conductive surface, the HOMO of both OPE variants could be directly imaged. DFT calculations confirmed that hybridization of molecular orbitals with the surface states is weaker for occupied orbitals than for unoccupied orbitals of the molecule. The recorded shapes of the HOMO were compared to DFT calculations of the molecules in the gas phase and good agreement was found. By employing low bias voltages the chemical structure of both molecules was directly imaged. Such a contrast mode is unusual for STM measurements and its origin is still under discussion. In order to measure the molecular conductance, we succeeded in partly lifting the molecules off the surface by pulling back the anchor group with the STM tip. The maximum obtainable lift height is typically 5 Å, before the molecule disconnects from the STM tip and falls back to the surface. Approaching this maximum detachment, we observe resistance values of ≈ 50 M Ω at 300 mV bias which is in good agreement with experimental values for similar molecules ([43]) but considerably lower than the average resistance of 90 G Ω for OPE-A in previous contacting experiments with carbon nanotube nanogap electrodes [21]. Since only a small part of the molecule is lifted (total length of the molecules is ≈ 50 Å) the resistance of the whole length of a single molecule suspended between two electrodes is expected to be much higher than the value observed here. The electron transport through large molecules is not only determined by the chemical configuration of the molecular backbone, but also indirectly by the conformation of the side groups. We presented a detailed investigation of the electron-induced switching between two metastable conformations of the alkyl chains attached to each side of the phenylene groups. We identified the underlying mechanism as a single electron process with an energy of about 300 meV. The switching between two bistable states provides the possibility to store information, using each alkyl chain as a memory bit. In summary, our results indicate that a high level of scrutiny on designated molecular building blocks is necessary before any complex systems are considered. By providing detailed insights into the electronic and atomic structure of two OPE molecules, this STM study will help understanding and subsequent tailoring the properties of future molecular electronic devices.

Acknowledgments

We acknowledge support by the DFG Center for Functional Nanostructures and Deutsche Forschungsgemeinschaft and Open Access Publishing Fund of Karlsruhe Institute of Technology.

References

- [1] Moroni M, le Moigne J and Luzzati S 1994 *Macromolecules* **27** 562
- [2] Tour JM, Jones LI, Pearson DL, Lamba JS, Burgin TP, Whitesides GM, Allara DL, Parikh AN and Atre SV 1995 *J. Am. Chem. Soc.* **117** 9529
- [3] Bunz UHF, Rubin Y and Tobe Y 1999 *Chem. Soc. Rev.* **28** 107
- [4] Tour JM et al 2001 *Chem. Eur. J.* **7** 5118
- [5] Zhao D and Moore JS 2003 *Chem. Commun.* **807**
- [6] Bunz UHF 2000 *Chem. Rev.* **100** 1605
- [7] Maya F, Flatt AK, Stewart MP, Shen DE and Tour JM 2004 *Chem. Mater.* **16** 2987
- [8] Jester S-S, Shabelina N, le Blanc SM and Höger S 2010 *Angew. Chem., Int. Ed. Engl.* **49** 6101
- [9] Jester S-S, Idelson A, Schmitz D, Eberhagen F and Höger S 2011 *Langmuir* **27** 8205
- [10] Reichert J, Ochs R, Beckmann D, Weber HB, Mayor M and Löhneysen H v 2002 *Phys. Rev. Lett.* **88** 176804

- [11] Weber H, Reichert J, Weigend F, Ochs R, Beckmann D, Mayor M, Ahlrichs R and Löhneysen H v 2002 *Chem. Phys.* **281** 113
- [12] Dhirani A-a, Zehner R W, Hsung R P, Guyot-Sionnest P and Sita L R 1996 *J. Am. Chem. Soc.* **118** 3319
- [13] Bumm L A, Arnold J J, Cygan M T, Dunbar T D, Burgin T P, Jones L II, Allara D L, Tour J M and Weiss P S 1996 *Science* **271** 1705
- [14] Cygan M T, Dunbar T D, Arnold J J, Bumm L A, Shedlock N F, Burgin T P, Jones L II, Allara D L, Tour J M and Weiss P S 1998 *J. Am. Chem. Soc.* **120** 2721
- [15] Gong J-r, Zhao J-l, Lei S-b, Wan L-j, Bo Z-s, Fan X-l and Bai C-l 2003 *Langmuir* **19** 10128
- [16] Mu Z, Yang X, Wang Z, Zhang X, Zhao J and Bo Z 2004 *Langmuir* **20** 8892
- [17] Kim S-U, Kim B-S, Park J-C, Shin H-K and Kwon Y-S 2006 *Curr. Appl. Phys.* **6** 608
- [18] Mössinger D, Jester S-S, Sigmund E, Müller U and Höger S 2009 *Macromolecules* **42** 7974
- [19] Seminario J M, Zacarias A G and Tour J M 2000 *J. Am. Chem. Soc.* **122** 3015
- [20] Lu J-Q, Wu J, Chen H, Duan W, Gu B-L and Kawazoe Y 2004 *Phys. Lett. A* **323** 154
- [21] Thiele C et al 2014 *Appl. Phys. Lett.* **104** 103102
- [22] Vonlanthen D, Mishchenko A, Elbing M, Neuburger M, Wandlowski T and Mayor M 2009 *Angew. Chem., Int. Ed. Engl.* **48** 8886
- [23] Lukas M, Dössel K, Schramm A, Fuhr O, Stroh C, Mayor M, Fink K and Löhneysen H v 2013 *ACS Nano* **7** 6170
- [24] Gotovac S, Hattori Y, Noguchi D, Miyamoto J-I, Kanamaru M, Utsumi S, Kanoh H and Kaneko K 2006 *J. Phys. Chem. B* **110** 16219
- [25] Gotovac S, Yang C-M, Hattori Y, Takahashi K, Kanoh H and Kaneko K 2007 *J. Colloid Interface Sci.* **314** 18
- [26] Grunder S, Muñoz Torres D, Marquardt C, Błaszczak A, Krupke R and Mayor M 2011 *Eur. J. Org. Chem.* **2011** 478
- [27] Marquardt C W, Grunder S, Błaszczak A, Dehm S, Hennrich F, Löhneysen H v, Mayor M and Krupke R 2010 *Nat. Nanotechnology* **5** 863
- [28] TURBOMOLE V6.4 2012 1989–2007 TURBOMOLE GmbH, since 2007 (www.turbomole.com)
- [29] Hehre W J, Ditchfield R and Pople J A 1972 *J. Chem. Phys.* **56** 2257
- [30] Becke A D 1993 *J. Chem. Phys.* **98** 5648
- [31] Li Y, Zhao J and Yin G 2007 *Comput. Mater. Sci.* **39** 775
- [32] Majumder C, Briere T, Mizuseki H and Kawazoe Y 2002 *J. Phys. Chem. A* **106** 7911
- [33] Becke A D 1988 *Phys. Rev. A* **38** 3098
- [34] Perdew J P 1986 *Phys. Rev. B* **33** 8822
- [35] Schäfer A, Horn H and Ahlrichs R 1992 *J. Chem. Phys.* **97** 2571
- [36] Eichkorn K, Weigend F, Treutler O and Ahlrichs R 1997 *Theor. Chim. Acta.* **97** 119
- [37] Grimme S, Antony J, Ehrlich S and Krieg H 2010 *J. Chem. Phys.* **132** 154104
- [38] Grimme S, Ehrlich S and Goerigk L 2011 *J. Comput. Chem.* **32** 1456
- [39] Samori P, Francke V, Enkelmann V, Müllen K and Rabe J P 2003 *Chem. Mater.* **15** 1032
- [40] Chen W, Madhavan V, Jamneala T and Crommie M F 1998 *Phys. Rev. Lett.* **80** 1469
- [41] Bürgi L, Brune H and Kern K 2002 *Phys. Rev. Lett.* **89** 176801
- [42] Jung T A, Schlittler R R, Gimzewski J K, Tang H and Joachim C 1996 *Science* **271** 181
- [43] Lu Q, Liu K, Zhang H, Du Z, Wang X and Wang F 2009 *ACS Nano* **3** 3861
- [44] Gross L, Mohn F, Moll N, Liljeroth P and Meyer G 2009 *Science* **325** 1110
- [45] de Oteyza D G et al 2013 *Science* **340** 1434
- [46] Temirov R, Soubatch S, Neucheva O, Lassise A C and Tautz F S 2008 *New J. Phys.* **10** 053012
- [47] Weiss C, Wagner C, Kleimann C, Rohlfing M, Tautz F S and Temirov R 2010 *Phys. Rev. Lett.* **105** 086103
- [48] Weiss C, Wagner C, Temirov R and Tautz F S 2010 *J. Am. Chem. Soc.* **132** 11864
- [49] Martinez J I, Abad E, González C, Flores F and Ortega J 2012 *Phys. Rev. Lett.* **108** 246102
- [50] Takács A F, Witt F, Schmaus S, Balashov T, Bowen M, Beaurepaire E and Wulfhekel W 2008 *Phys. Rev. B* **78** 233404
- [51] Schmaus S, Bagrets A, Nahas Y, Yamada T K, Bork A, Bowen M, Beaurepaire E, Evers F and Wulfhekel W 2011 *Nat. Nano* **6** 185
- [52] Venkataraman L, Klare J E, Nuckolls C, Hybertsen M S and Steigerwald M L 2006 *Nature* **442** 904
- [53] Das B 2010 *Nanotechnology* **21** 395201
- [54] Eigler D M, Lutz C P and Rudge W E 1991 *Nature* **352** 600
- [55] Brandbyge M and Hedegård P 1994 *Phys. Rev. Lett.* **72** 2919
- [56] Gao S, Persson M and Lundqvist B I 1997 *Phys. Rev. B* **55** 4825
- [57] Stipe B, Rezaei M, Ho W, Gao S, Persson M and Lundqvist B 1997 *Phys. Rev. Lett.* **78** 4410
- [58] Donhauser Z J et al 2001 *Science* **292** 2303
- [59] Elste F, Weick G, Timm C and Oppen F 2008 *Appl. Phys. A* **93** 345
- [60] Liljeroth P, Repp J and Meyer G 2007 *Science* **317** 1203
- [61] Tikhodeev S and Ueba H 2004 *Phys. Rev. B* **70** 125414
- [62] Demuth J E, Ibach H and Lehwald S 1978 *Phys. Rev. Lett.* **40** 1044